NASA TECHNICAL TRANSLATION NASA TT F-16,112

STRUCTURE AND DYNAMICS OF THE THERMOSPHERE OF VENUS

M. N. Izakov and S. K. Morozov

Translation of "Struktura i dinamika termosfery venery". Institute of Cosmic Studies, Academy of Sciences USSR, Report No. PR-176, Moscow, 1974, 32 pp.

NATIONAL AERONAUTICS AND SPACE ADMINISTRATION
WASHINGTON, D. C. 20546 JANUARY 1975

STANDARD TITLE PAGE

1. Report No.	2. Government Accession No.	3. Recipient's Catalog No.
NASA TT F-16,112		

4. Title and Subtitle	5. Report Date
STRUCTURE AND DYNAMICS OF THE THERMOSPHERE OF VENUS	January 1975
	6. Performing Organization Code

7. Author(s)	8. Performing Organization Report No.
M. N. Izakov and S. K. Morozov	
	10. Work Unit No.

9. Performing Organization Name and Address	11. Contract or Grant No.
SCITRAN Box 5456 Santa Barbara, CA 93108	NASw-2483
	13. Type of Report and Period Covered
	Translation
12. Sponsoring Agency Name and Address National Aeronautics and Space Administration Washington, D.C. 20546	14. Sponsoring Agency Code

15. Supplementary Notes

Translation of "Struktura i dinamika termosfery venery". Institute of Cosmic Studies, Academy of Sciences USSR, Report No. PR-176, Moscow, 1974, 32 pp.

16. Abstract

The temperature, density, and velocity distributions of macroscopic motion in the Venus thermosphere are calculated, taking into account their interreactions of altitudes of 110 - 210 km for moderately high solar activity. It is shown that the absorption of solar radiation on the diurnal (daylight) side causes a global circulation with vertical upward motion on the diurnal side, and downward on the nocturnal side with velocities of several meters per second, and with horizontal velocities up to several hundred m/sec away from the subsolar point in the upper thermosphere. The temperature distribution in the Venus thermosphere is characterized by a temperature drop from day to night of 800° K at the subsolar point, to 300° K at the antisolar points. The calculated temperatures are close to the experimental ones if the variability of the temperature with solar activity is taken into account.

17. Key Words (Selected by Author(s))	18. Distribution Statement
	Unclassified - Unlimited

19. Security Classif. (of this report)	20. Security Classif. (of this page)	21. No. of Pages	22. Price
Unclassified	Unclassified	27	

ANNOTATION

The temperature, density and velocity distributions of macroscopic motion in Venus thermosphere are calculated, taking into account their interreaction at altitudes of 110 - 210 km for moderately high solar activity. It is shown that the absorption of solar radiation on the diurnal (daylight) side causes a global circulation with vertical upward motion on the diurnal side, and downward motion on the nocturnal side with velocities of several meters per second, and with horizontal velocities of up to several hundred meters per second away from the subsolar point in the upper thermosphere. The temperature distribution in the Venus thermosphere is characterized by a temperature drop from day to night of 800° K at the subsolar point, to 300° K at the antisolar points. The calculated temperatures are close to the experimental ones if the variability of the temperature with solar activity is taken into account.

STRUCTURE AND DYNAMICS OF THE THERMOSPHERE OF VENUS

M. N. Izakov and S. K. Morozov

Introduction

The thermosphere of a planet is defined as the region of the upper atmosphere where the thermal conditions are determined by the absorption of short wavelength solar radiation (ultraviolet and x-radiation), and by gas thermal conduction. In its lower part, conditions are also determined by the infrared thermal radiation of the atmosphere. Here, the temperature increases with altitude, and then becomes isothermal. On Venus, the thermosphere is distributed at altitudes above 120 - 130 km. Solar radiation absorption on the diurnal side causes a significant difference between daytime and nighttime temperatures, and causes macroscopic global motion in the thermosphere. /3*

Data on Venus upper atmosphere occupies an important place among the data on its atmosphere, which were obtained recently from satellites [1 - 3, for example]. Thus, the distribution of the hydrogen concentration with altitude was obtained from measurements of

*Numbers in the margin indicate pagination in the original foreign text.

scattered Lyman-alpha hydrogen radiation. These measurements were made by "Venus-4" [4 - 5] on the nocturnal side of the planet, and by "Mariner-5" [6 - 8] on the diurnal side. The temperature of the upper atmosphere was calculated from these profiles. The distribution of electron concentration with altitude was obtained from the refraction of radio waves from "Mariner-5" as it approached and then emerged from behind the planet [9 - 12]. The temperature of the upper thermosphere was also determined from these measurements [13, 14]. /4

Empirical models of Venus atmosphere were constructed by generalizing the experimental data [15, 16, 26]. The first theoretical models of the thermosphere were constructed by interpreting the empirical data by trying to understand the mechanisms which control the temperature distribution in the thermosphere [17 - 25]. Our work is devoted to constructing a theoretical model of Venus thermosphere, which is free of several unjustified simplifications which were used in previous models. It is related to our work on modeling the Earth's thermosphere [30 - 31].

1. Statement of the Problem

1.1. Basic Equations

A planet's thermosphere can be considered to be a continuous medium up to high altitudes, and the Navier-Stokes gas dynamic equations can be used to describe it (for regions where the ratio of the molecular mean free path to the altitude scale is less than unity [27 - 29]). The thermosphere of a planet is a thin gas layer, in which the ratio of the characteristic vertical dimension (altitude scale) to the characteristic horizontal dimension (planet radius) is on the order of 10^{-2}. It can be shown [27 - 29] that for global processes in this thin layer, the Navier-Stokes equation can be transformed, so that the equation for horizontal motion and the energy equation reduce to the corresponding equations for boundary-layer theory. The equation for vertical motion transforms to the

quasi-static equation (barometric equation). By considering these transforms, it is possible to talk of using the "boundary-layer approximation". The main difference here is that the density and the transfer coefficients change by several orders of magnitude along the vertical axis. /5

It is convenient to examine two variants of the model: a) with a non-rotating mesosphere, and b) with a mesosphere that rotates with a period of 4 terrestrial days in the same direction as the planet.

a) Variant with a non-rotating mesosphere

Because of the very slow rotation of Venus around its axis, a solar day on Venus is approximately 118 Earth days. On the other hand, the characteristic time for establishing a thermal balance and a macroscopic circulation is several days. Thus we can neglect the rotation of Venus and consider a problem which is symmetric along a line from Venus to the sun.

We choose a spherical coordinate system with its center at the center of the planet. The axis $\theta = 0$ is directed toward the sun. Because of symmetry, $V_\phi = 0$ and $\partial/\partial\phi = 0$. The basic system of equations for continuity, energy, inertia, quasi-statics, and state has the form:

$$\frac{\partial \rho}{\partial t} + \frac{\partial}{\partial r}(\rho V_r) + \frac{1}{r_0 \sin\theta}\frac{\partial}{\partial \theta}(\sin\theta \rho V_\theta) = 0; \quad (1)$$

$$C_v \rho\left(\frac{\partial T}{\partial t} + V_r\frac{\partial T}{\partial r} + \frac{V_\theta}{r_0}\frac{\partial T}{\partial \theta}\right) + p\left(\frac{\partial V_r}{\partial r} + \frac{1}{r_0 \sin\theta}\frac{\partial \sin\theta V_\theta}{\partial \theta}\right) - \frac{\partial}{\partial r}\left(\varkappa \frac{\partial T}{\partial r}\right) - \eta\left(\frac{\partial V_\theta}{\partial r}\right)^2 = Q_{ST} - Q_{1R}; \quad (2)$$

$$\rho\left(\frac{\partial V_\theta}{\partial t} + V_r\frac{\partial V_\theta}{\partial r} + \frac{V_\theta}{r_0}\frac{\partial V_\theta}{\partial \theta} + \frac{V_r V_\theta}{r_0}\right) - \frac{\partial}{\partial r}\left(\eta \frac{\partial V_\theta}{\partial r}\right) = -\frac{1}{r_0}\frac{\partial p}{\partial \theta}; \quad (3)$$

$$\frac{\partial p}{\partial r} = \rho g; \quad (4)$$

$$p = \rho R_0 T/m, \quad (5)$$

where t is time; ρ, T, P, m are the density, temperature, pressure and molecular weight of the gas; V_r, V_θ are the velocity components; η, $\varkappa$ are the coefficients of viscosity and thermal conductivity; Q_{ST} and Q_{1R} are the heat source and sink defined below. /6

It can be assumed [21, 25] that the main component of the Venus thermosphere is CO_2, since M = 44. Since a thin layer Δr = 100 km is being considered, it is possible to take g = 830 m/sec^{2}m and replace r in the equations by r_0 = 6150 km. We also use $C_v = 6 \cdot 10^6$ erg/g-°K, $\eta = 1.4 \cdot 10^{-4}$ g/cm-sec, and $\varkappa = 1.5 \cdot 10^3$ erg/cm-sec-°K.

Here, we neglect ionic friction, as compared to the model of the Earth's thermosphere [30, 31]. This is possible since the Venus weak magnetic field [32, 33] makes the ionic gyrofrequency much smaller than the ion-neutral collision frequency. Thus there is not much difference in the velocities of ions and neutral particles.

The possible presence of turbulence in the lower thermosphere is not considered.

b) Variant with a four-day rotating mesosphere

The Venus mesosphere at altitudes of 70 - 80 km rotates with a period of 4 terrestrial days (at the lower latitudes) in the same direction as the planet [47]. This rotation should be transmitted into the thermosphere through viscosity. Considering the rotation makes the problem three-dimensional; however, in the first stage of the investigation, we only consider the thermosphere in the equivalent region, which lets us return to the two-dimensional problem.

We choose a static spherical coordinate system with the center at the center of the planet, and the $\vartheta = 0$, $\phi = 0$ axes along a line from the planet to the Sun (θ is latitude, and ϕ is longitude) computed from the subsolar point in the direction of the planet's rotation). We will examine the thermosphere in the equatorial plane $\theta = 0$. This is a satisfactory approximation, since the symmetry of the problem with respect to the equator makes it possible to take $v_\theta = 0$ for $\theta = 0$ (because of the small inclination of the plane of the equator to the orbital plane of Venus). We assume here also $\partial v_\theta / \partial \theta = 0$. In analogy with the Earth's thermosphere [30, 31], it

/7

can be assumed that this approximation does not introduce any substantial error. We also make the same simplifications as in the first variant, and obtain the system of equations:

$$\frac{\partial \rho}{\partial t} + \frac{\partial}{\partial r}(\rho v_r) + \frac{1}{r_0}\frac{\partial}{\partial \varphi}(\rho v_\varphi) = 0 \qquad (1a)$$

$$c_v \rho \left(\frac{\partial T}{\partial t} + v_r \frac{\partial T}{\partial r} + \frac{v_\varphi}{r_0}\frac{\partial T}{\partial \varphi}\right) + p\left(\frac{\partial v_r}{\partial r} + \frac{1}{r_0}\frac{\partial v_\varphi}{\partial \varphi}\right) - \frac{\partial}{\partial r}\left(\varkappa \frac{\partial T}{\partial r}\right) - \eta\left(\frac{\partial v_\varphi}{\partial r}\right)^2 = \qquad (2a)$$

$$\rho\left(\frac{\partial v_\varphi}{\partial t} + v_r \frac{\partial v_\varphi}{\partial r} + \frac{v_\varphi}{r_0}\frac{\partial v_\varphi}{\partial \varphi}\right) - \frac{\partial}{\partial r}\left(\eta \frac{\partial v_\varphi}{\partial r}\right) = -\frac{1}{r_0}\frac{\partial p}{\partial \varphi}; \qquad = Q_{3T} - Q_{1R} \qquad (3a)$$

Equations 4 and 5 are included in the above system without change.

1.2. Heat Source and Sink

The heat source in the planet's thermosphere is the ultraviolet and x-ray solar radiation, which is absorbed and causes dissociation and photo-ionization, with part of the photon energy being transformed into heat [34 - 35]. Considering the predominance of CO_2 in the Venus thermosphere yields a function of the form:

$$Q_{ST}(r) = \int_{30\text{Å}}^{302\text{Å}} \varepsilon_u F(\lambda, r) n \sigma^u(\lambda) d\lambda + \int_{650\text{Å}}^{2000\text{Å}} \varepsilon_D F(\lambda, r) n \sigma^D(\lambda) d\lambda, \qquad (6)$$

where

$$F(\lambda, r) = F(\lambda, \infty) \exp(-\sigma(\lambda) n H Ch), \qquad (7)$$

$\sigma^u, \sigma^D, \sigma$ are the cross sections for ionization, dissociation, and total absorption; n, H are the concentration and altitude scale of CO_2; ε_u and ε_D are the thermal production efficiencies for ionization and dissociation, that is, the fraction of the photon energy that is transformed into heat; $F(\lambda, r)$, $F(\lambda, \infty)$ are the spectral solar radiation currents (erg/cm^2 sec Å) at a given altitude and at the boundary of the atmosphere; and Ch is the Chapman function. For actual calculations, $\varepsilon_u = 0.3$, $\varepsilon_D = 0.3$. It was shown [35] that ε_D changes with altitude, but that $\varepsilon_D = 0.3$ at altitudes where most dissociative absorption takes place. The value $\varepsilon_u = 0.3$ was obtained [37] by comparing calculated and measured electron concentration profiles.

The solar radiation flux was taken from [42, 43], and the cross section — from [36]. For convenience, the Function (6) can be approximated by the formula:

$$q_{s\infty} = \frac{Q_{st}}{\beta} = \sum A_i \exp(-B_i \beta T Ch), \quad (8)$$

where A_i and B_i are expressed in terms of the average cross section and average current, and i = 1.2.

The heat sink emission of infrared radiation in the 15 micron band from CO_2 was taken for an optically thin layer in the form [28, 38, 39]:

$$Q_{ie} = E n^2 \eta^B \exp(-E/\kappa T) \varphi(\chi) \quad \left[\frac{\text{erg}}{\text{cm}^3\text{-sec}}\right] \quad (9)$$

where η^B is the vibrational relaxation parameter of the 15 micron band of CO_2: and $\phi(x)$ is the screening function:

$$\eta^0 = 8{,}3 \cdot 10^{-15} T \exp\left(-\frac{40\,\delta}{T^{1/3}}\right), \quad \left[\frac{cm^3}{cek}\right], \quad (10)$$

and $\phi(x)$ is the screening function:

$$\varphi(\chi) = 1 - (1+\chi)\exp(-\chi) \qquad \chi = \frac{2 \cdot 7 \cdot 10^9}{n}\left(1 + \frac{A}{n\eta^B}\right)$$
$$E = 1{,}32 \cdot 10^{-13} \text{ erg} \qquad \kappa = 1{,}38 \cdot 10^{-16} \text{erg}/^\circ\text{K} \quad (11)$$

A is the Einstein coefficient (A^{-1} = 0.37 sec). /9

Comparison with Dickinson's infrared radiation transport calculations [40, 41] shows that Equation (9) gives sufficient accuracy for our model.

Since the smallest period of regular change of the solar flux $F(\lambda, \infty)$ is roughly 27 days (the rotation period of the Sun around its axis), we take $Q_{st}(r, \theta)$ as a constant, seek a stationary solution to the system (1 - 5), and consider the process fixed in time.

1.3. Boundary and Initial Conditions

The basic system of equations (1 - 5) is a system of four differential equations, two of second order and two of first order in r, so that it is necessary to postulate six boundary conditions for r. At the upper boundary $r = r_1$, there are three conditions, which come from the natural requirements that no heat, momentum, or mass escape from the atmosphere*:

$$\frac{\partial T}{\partial r}(r_1, \theta) = 0; \quad \frac{\partial v_\theta}{\partial r}(r_1, \theta) = 0; \quad \frac{\partial^2 v_r}{\partial r^2}(r_1, \theta) = 0. \qquad (12)$$

The choice of a lower boundary and the condition on it will be discussed below.

We choose the lower boundary to be at an altitude of 110 km, mainly because the solar ultraviolet source q_{ST} is negligibly small at that altitude, as can be seen from calculations using the formulas presented above. As a result, variations in temperature and density /10 along the horizontal should also be small. This is shown by results obtained in radio eclipse experiments on "Mariner-5", where no differences between day and night temperatures were found on the planet for altitudes up to 90 km [10, 12].

On the other hand, the boundary can be placed at 110 km, since the calculated results will show that the thermospheric vortex closes above this boundary

Naturally, we would like to drop the lower boundary, to the level of the upper boundary of the Venusian clouds, for instance. However, this would greatly complicate the calculations for two reasons. First, the approximation of an optically thin layer would not be accurate enough for computing the infrared sink at the lower

*For an examination of the asymptotic solution and the choice of the condition $\frac{\partial^2 v_r}{\partial r^2} = 0$ from the requirement of zero mass flux at infinity, see [30].

altitudes, so that here the complete radiation transport equation would have to be used [40, 41]. Second, decreasing the altitude increases the probability of descending into the lower turbulent region, since the turbulent characteristics in the upper Venusian atmosphere are not yet completely known.

From the above discussion, we set:

$$T(r_0, \theta) = T_0 = 200^\circ K, \quad \rho(r_0, \theta) = \rho_0 = 1{,}3 \cdot 10^{-3} \text{ g/cm}^3 \tag{13}$$

at the lower boundary. The numerical values of T_0, ρ_0 are taken close to the values of the model [26].

Furthermore, in variant "a" (non-rotating mesosphere), we set:

$$v_\theta(r_0, \theta) = 0 \tag{13a}$$

and in variant "b" (4-day rotation):

$$\langle v_\varphi(r_0, \varphi) = \Omega r_0 \rangle = 100 \text{ m/sec} \tag{13b}$$

Because of axial symmetry, the problem can be examined in the half ring between $\theta = 0$ and $\theta = \pi$: /11

$$\frac{\partial T}{\partial \theta}(r) = 0, \quad \frac{\partial \rho}{\partial \theta}(1) = 0, \quad v_\theta(r) = 0. \tag{14}$$

The starting data for variant "a" is the solution for the one-dimensional model with a global average heat source $\bar{Q}_{ST} = \frac{1}{2} Q_{ST}(\theta = \frac{\pi}{3})$. In variant "b", we add $v_\varphi(r, \varphi) = 100$ m/sec at $t = 0$.

1.4. Computational Algorithm

The computational method is a development of the method given in [30]. We note that the nonstationary nature of the calculational problem consists of two parts. The first is the change of the density and the kinematic transfer coefficients by several orders of magnitude along the vertical. The second is the spatial periodicity

of the problem, in which perturbations die out. The initial system (1 - 5) is rewritten in terms of the variables $\vartheta = \ln \rho/\rho_0$, T, v_θ, v_r. For a numerical solution, the differential equations were replaced by difference equations. A two-point t^n, t^{n+1} difference method was used, which was implicit in r, and implicit but iteratively soluble in θ. This method allows us to reduce the problem solution for a given iteration to the solution of boundary problems in r for a fixed θ. The first-order derivatives were approximated from two points, and the second-order derivatives — from three. All derivatives were taken from the upper layer. Nonlinear difference equations (*) were solved iteratively at each layer t^{n+1}. Iterations over nonlinearities were combined with iterations on θ. The one-dimensional linear boundary problem on the ray θ = const was solved by the method /12 of elimination by choosing the maximum element in the column. The zones in r were not constant, but decreased in size with increasing r. Calculations used 13 zones in θ, and 21 zones in r (in variant "b", there were 22 zones in φ).

3. Results of the Calculations

Calculations were made with the model for conditions of moderately high solar activity (corresponding to a solar radiation flux at a 10.7 cm wavelength of $F_{10.7} = 150 \cdot 10^{-22}$ V/m^2 Hz), for which there are experimental data on the flux of short wavelength solar radiation F_λ [42]. In the calculations, the solution of the one-dimensional thermal conduction model for a globally averaged source was used as the initial data, and the stationary regime was reached after a time on the order of 3 to 5 Earth days.

Figure 1 shows the quantity $q = q_{ST} - q_{12}$ as a function of the angle θ (1a), and of altitude h (1b). It should be noted that the vertical scales are different above and below zero. The dot-dashed

*Translator's note. Illegible in the original foreign text.

curve was taken from a curve for the globally averaged source $\bar{q} = \frac{1}{2} q_{ST}(\theta = \frac{\pi}{3}) - q_{1R}$.

a) Variant with a non-rotating mesosphere

Figure 2 shows the temperature distribution with angle θ (2a) and altitude h (2b). The basic feature of the temperature distribution of the upper atmosphere T_∞ (in the isothermal region) is the large difference of daytime and nighttime temperatures (T_∞ = 800° K at the subsolar point, and T_∞ = 300° K at the opposite solar point). The transition zone with the larger horizontal gradient is placed within a rather narrow zone near the terminator. The broken curve corresponds to the variant $\vec{V} = 0$, i.e., the one-dimentional conduction model with a θ-dependent thermal contribution. It can be seen that the winds substantially reduce the contrast on the diurnal and nocuurnal sides; in their absence, the difference would be higher by several hundred degrees. The altitudinal temperature profile (Figure 2b) reaches a plateau near 190 km at the subsolar point, and near 120 km on the nocturnal side. The non-monotonic nature of the temperature variation with altitude h should be noted at the lower portion of the curve. The minimum temperature at $\sim$ 130 km is caused by a maximum in the infrared sink q_{1R}, so that this non-monotonic behavior is not a result of some error in the approximation for q. The broken curve corresponds to the temperature corresponding to a one-dimensional thermal conduction model with a globally averaged source. /13

Figure 3 shows the distribution density with angle θ (3a), and with altitude h (3b).

Figure 4 shows the horizontal component of the velocity v_θ. It can be seen that the wind velocity exceeds 100 m/sec in a large part of the thermosphere, with a maximum of $\sim$ 400 m/sec near the terminator.

In the lower thermosphere at altitudes of 110 - 130 km, there is a reverse flow region from the nocturnal to diurnal side. The velocity here is not large. However, the mass flux ρv_θ is significant, so that the total flux through a section θ = constant is close to zero for any θ. The vertical scales in Figure 4b are significantly different above and below the abscissa. /14

Figure 5 shows the vertical velocity component v_r. It can be seen that v_r is upwards on most of the daytime side, and has a value of 1 m/sec in the upper thermosphere near the subsolar and antisolar points, and reaches 4 m/sec near the terminator.

Figure 6 shows the velocity field in the Venusian thermosphere (the vertical scale is 200 times larger than the horizontal scale). The altitude region below 130 km is shown in a scale 20 times larger than that used for higher altitudes.

In order to determine the role of the lower boundary conditions, calculations were performed with a lower boundary placed at 120 km under the condition that $T = T_0$ from 110 to 120 km. The solution remained practically unchanged in the upper part. The vortices closed partially below the region of the calculations. A calculation was performed in which the condition $\frac{\partial v_\theta}{\partial r}(r_0, \theta) = 0$ replaced the condition $v_\theta = 0$ at the lower boundary. The solution was practically unchanged.

These numerical experiments substantiated the fact that the global phenomena in the thermosphere can be examined spearately from other atmospheric layers to a first approximation.

b) Variant with a four-day rotation

Figure 7 shows the temperature distribution with angle ϕ at altitudes of 200 and 152 km in the equatorial thermosphere of Venus.

For comparison, the broken curve was taken from an analogous distribution with no rotation, corresponding to variant "a". It can be /15
seen that the effect of the four-day rotation somewhat displaces the temperature curves for an altitude of 200 km, and increases the temperature near the terminator by 30 - 40°. The temperature remains practically unchanged at an altitude of 152 km.

Figure 8 shows the distributions of the horizontal velocity component v_ϕ and the vertical velocity component v_r with angle ϕ. Here, too, the broken curves are for v_θ and v_r from variant "a" (in the absence of rotation, so that the scale of v_θ is shifted by 100 m/sec relative to that for v_ϕ, since we wish to compare velocity after subtracting the rotation $v_\varphi - \Omega r_0$ with v_θ).

Comparison of variants "a" and "b" shows that adding a four-day rotation to the thermospheric winds shifts it in the direction of rotation and distorts it such that the velocity near the nocturnal terminator differs roughly by 100 m/sec, and by 200 m/sec near the antisolar point (naturally, the numerical values are approximate, since we neglected meridional flow in variant "b"). It is important to note that motion in most of the upper thermosphere is directed from the subsolar point to the antisolar point, independent of rotation. That is, the wind velocity exceeds the rotation velocity in a large region around the morning terminator.

The upward vertical velocity in variant "b" varies little from that of variant "a". The downward vertical velocity in "b" is somewhat higher than in "a", and its shape is somewhat displaced at the /16
antisolar point.

Using the values of T and h from the model, we find that the altitude of the thermopause or exosphere (where the mean free path equals the scale height) is approximately $h_e \simeq 200$ km at the subsolar point, and $h_e \simeq 150$ km at the antisolar point. This indicates that

use of the Navier-Stokes equations is not strictly valid at the higher altitudes that were investigated. However, the resulting errors are not large.

4. Discussion of the Results

An examination of the claculated results shows that there is a close interrelationship between the thermal conditions and the global motion in the Venus thermosphere. This indicates that it is impossible to construct a temperature and density distribution model of the Venus thermosphere without including this interrelationship, for example, by using the solution to the one-dimentional heat-conduction equation, as was done in several works.

We will compare the results we obtained with the available experimental data. The temperature of the upper thermosphere was computed to be $T_\infty \approx 300°$ [4, 5] from the altitude scale for hydrogen concentration, which was measured from the intensity of scattered Lyman-alpha radiation from hydrogen by "Venus-4" on the nocturnal side of the planet (for $\theta \approx 105°$). This result is very close to the data of our model.

The temperature T_∞ on the diurnal side of the planet (for $\theta \approx 45°$ K) was computed to be $T_\infty \approx 650°$ K from the electron altitude scale, which was measured by "Mariner-5" [9 - 12]. The result was measured during solar activity that corresponded to $F_{10.7} = 120 \cdot 10^{-22}$ V/m^2-Hz. The same value of T_∞ was obtained from the upper part of the hydrogen concentration profile, which was also measured by "Mariner-5" [6 - 8] (although some confusion remains, which is related to the lower part of this profile, see [44]). /17

The hydrogen profile, measured by "Mariner-10" [51] yielded a value $T_\infty \approx 400°$ K for $F_{10.7} = 75 \cdot 10^{-22}$ V/m^2 Hz. Our calculations yielded a value $T_\infty \approx 800°$ K for a solar ultraviolet flux, corresponding to $F_{10.7} = 150 \cdot 10^{-22}$ V/m^2 Hz, which is in good

agreement with experimental data, allowing for the dependence of T_∞ on the solar activity. It is interesting that the dependence of T_∞ on $F_{10.7}$ (as determined from these three points) is practically linear.

Since the temperature from the model corresponds with the experimental temperature, the value of the short wavelength solar radiation flux, used in the calculations, is sufficient for the observed thermospheric heating.

We computed a profile of the electron concentration (for photochemical equilibrium) from profiles of T and ρ that we obtained from the model. The calculated electron profiles were close to the experimental ones [11]; the maximum n_e was $5.5 \cdot 10^5$ cm^{-3} from experiment, and $4.5 \cdot 10^5$ cm^{-3} from the model; the altitudes for the maxima were 143 and 147 km, respectively.

Comparison of variant "a" of our model with Dickinson"s model [24, 25] shows that, aside from some similarities (similar temperatures T_∞ at the subsolar and antisolar points and maximum wind velocities), the models are quite substantially different. The main /18
differences of Dickinson's model from our model are as follows. His model has no reverse flow in the mesosphere up to 95 km. His has a completely different altitude profile of the horizontal wind velocity, with large velocities of 300 - 500 m/sec at 115 - 120 km, following a decrease at 130 - 135 km, and with new increases at higher altitudes. (The source of this wind increase in the lower thermosphere, where the heat source is negligibly small, from Figure 1b, is completely unclear.) His vertical velocities are much smaller, and are close to zero near the terminator, while our model has a maximum for the vertical velocities in the upper thermosphere near the terminator (Figure 5a). There are also differences in the spatial distributions of the temperature, although the temperature differences between the diurnal and nocturnal sides are similar, especially from [25], where $T_\infty \approx 700°$ at the subsolar point, and $T_\infty \approx 300°$ at the

antisolar point. We feel that Dickinson's model contains very strong limitations. First of all, he linearizes the equations and throws out terms of the type $(\vec{v}\nabla)\vec{v}$, which is not correct for the thermosphere, where variations in T, ρ, v are not small compared with their average values. Furthermore, he expands the solution functions in a spherical harmonic series and uses a small number of harmonics.

Since the reverse flow occurs at rather large altitudes, then the mass transfer hardly helps in the recombination of CO and O (as assumed in [25]). Without turbulent transfer, it is impossible to /19
explain the CO_2 in the thermosphere in the presence of fast photodissociation and slow recombination (see, for example, [45, 46]). However, aside from the noted deficiencies, Dickinson's model played an important role as the first model which attempted to evaluate the interaction of the thermal conditions and the motions in the Venus thermosphere.

Conclusions

The constructed model and the comparison of the model with experimental data indicates the following basic features of Venus thermosphere.

The temperature distribution is characterized by large differences of the upper thermospheric temperatures T_∞ between the diurnal and nocturnal sides of the planet: for moderately high solar activity, corresponding to $F_{10} = 150 \cdot 10^{-22}$ V/m^2 Hz, $T_\infty \simeq 800°$ K at the subsolar point, and $T_\infty \simeq 300°$ K at the antisolar point.

In the absence of rotation, the winds in the thermosphere form a single vortex, in which the gas rises on the diurnal side, transports in the upper atmosphere into the nocturnal side, then sinks and returns from the nocturnal side to the diurnal side in the upper mesosphere at an altitude range of 115 - 130 km, where the heat

source from short wavelength solar radiation is negligibly small. Here, the horizontal wind component in the upper thermosphere has a value of 100 - 400 m/sec, which increases toward the terminator, and is of the order of 10 m/sec in the reverse flow in the mesosphere. The vertical wind component is upward over most of the diurnal hemisphere, and downward on the nocturnal side. Its value is 1 - 4 m/sec in the upper thermosphere, and also has a maximum near the terminator. /20

A four-day rotation of the mesosphere is transmitted into the thermosphere and shifts the thermospheric vortex somewhat in the direction of rotation. The temperature and density distributions are changed slightly.

The model indicates a strong interaction of the thermal conditions and motions in the thermosphere. In particular, the vertical wind component operates as a noticeable local heat source and sink through adiabatic compression and expansion of the gas in the gravitational field.

Temperatures from the model agree with experimental data, taking into account the variation of the data with solar activity.

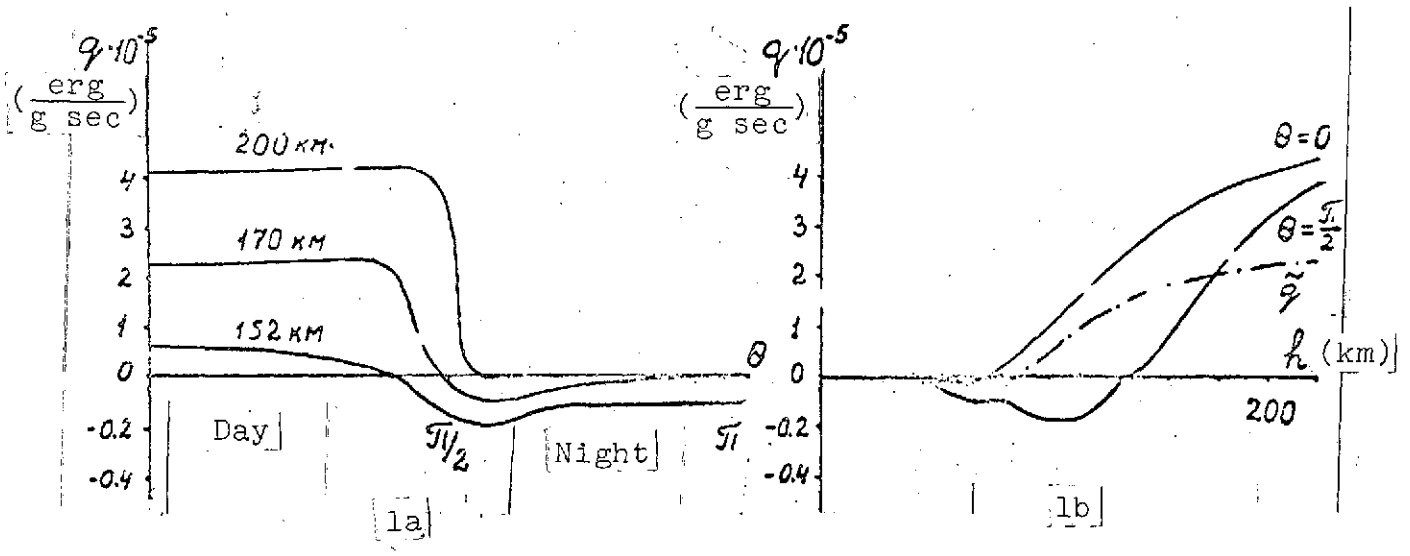

Figure 1. Distribution of the heat source of the Venus thermosphere q (erg/g-sec) with angle θ, and with altitude h. q is the globally averaged source. Scales are different for the positive and negative values of q

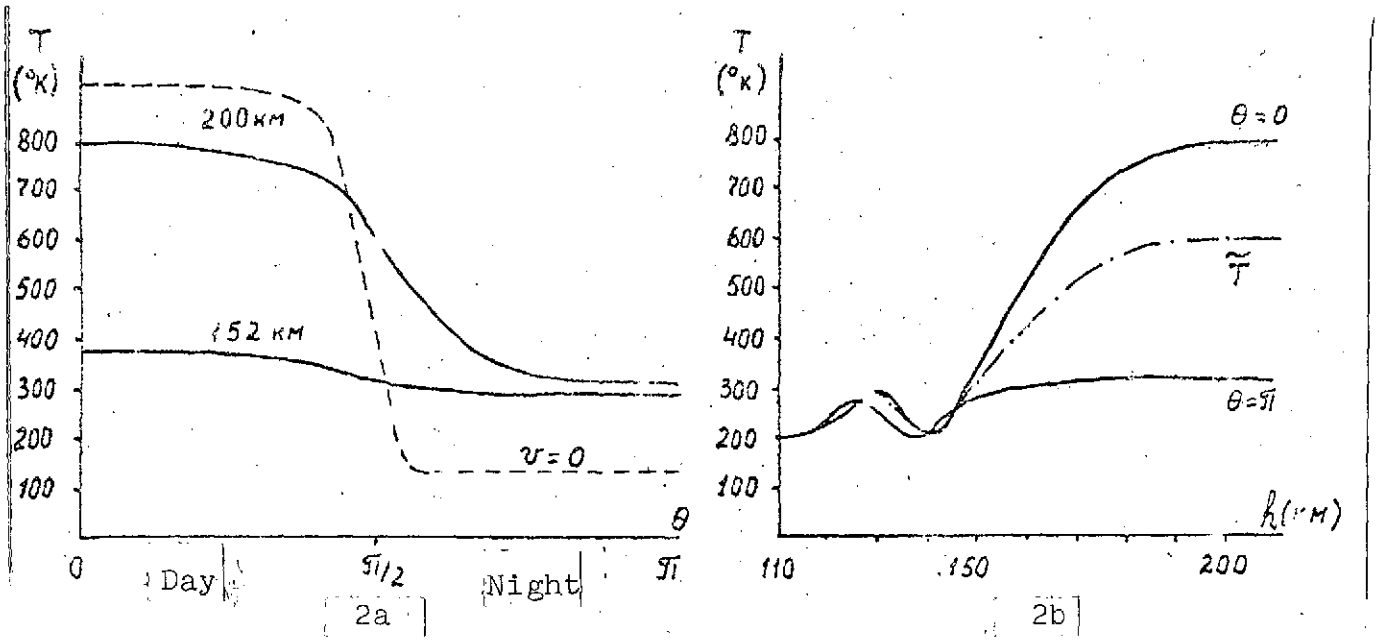

Figure 2. Distribution of temperature T in a non-rotating Venus thermosphere with angle θ and with altitude h. The dashed curve is for zero velocity. The dot-dashed curve is the global average

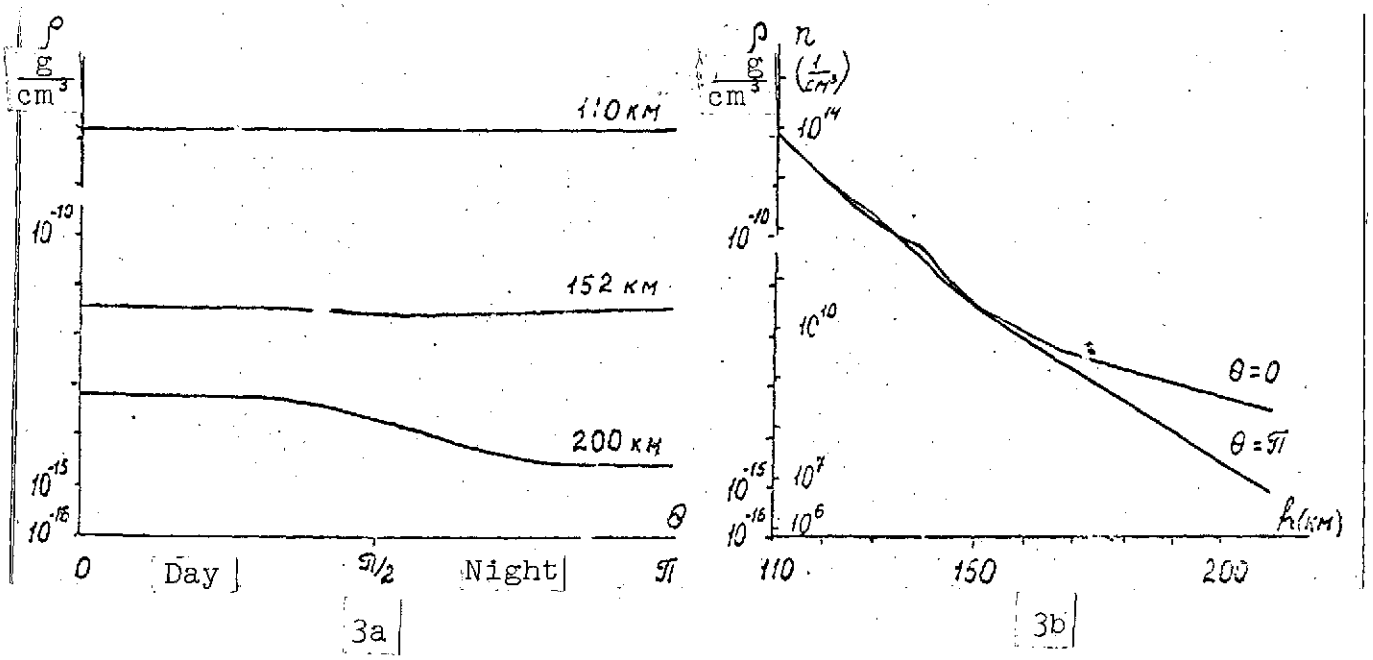

Figure 3. Distribution of the density ρ and concentration r in a non-rotating Venus thermosphere with angle θ and altitude h

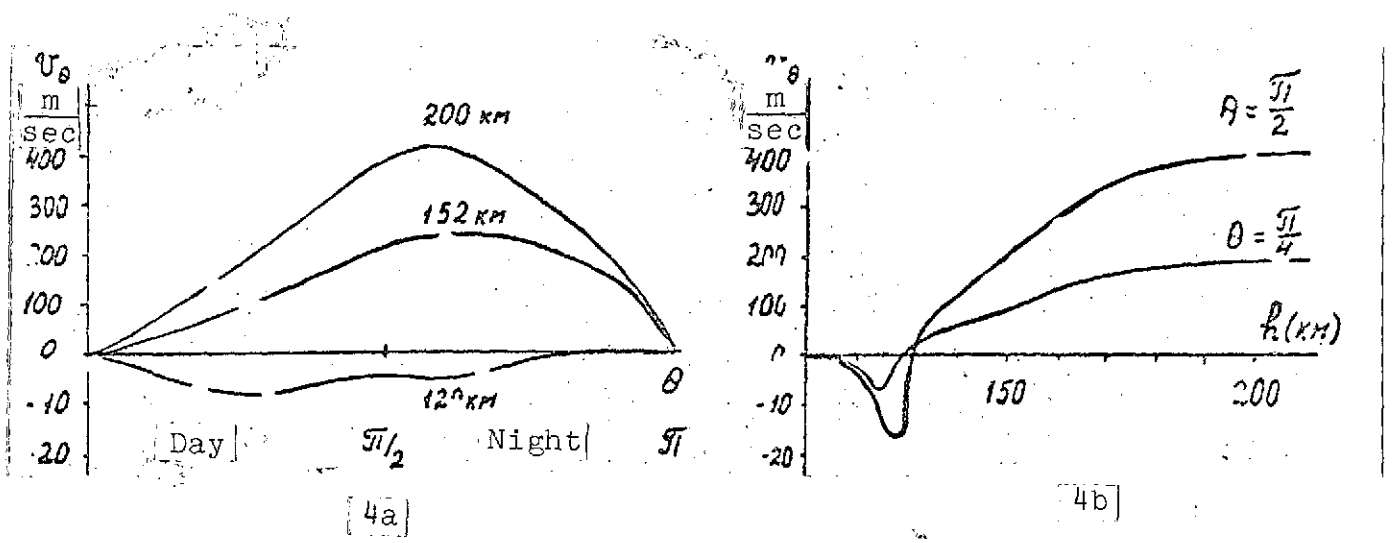

Figure 4. Distribution of the horizontal component of the wind velocity v_θ in a non-rotating Venus thermosphere with angle θ and altitude h. The scale is different for the positive direction (from the subsolar to antisolar points) and the negative direction

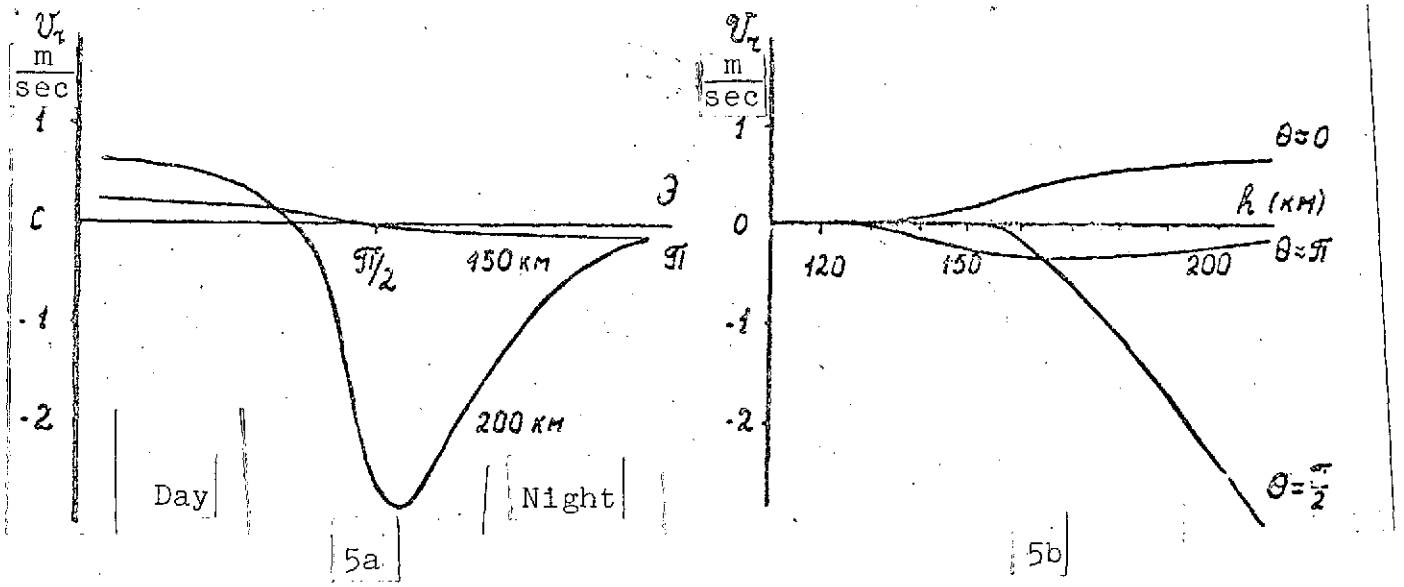

Figure 5. Distribution of the vertical component of the wind velocity v_r in a non-rotating Venus thermosphere with angle θ and altitude h

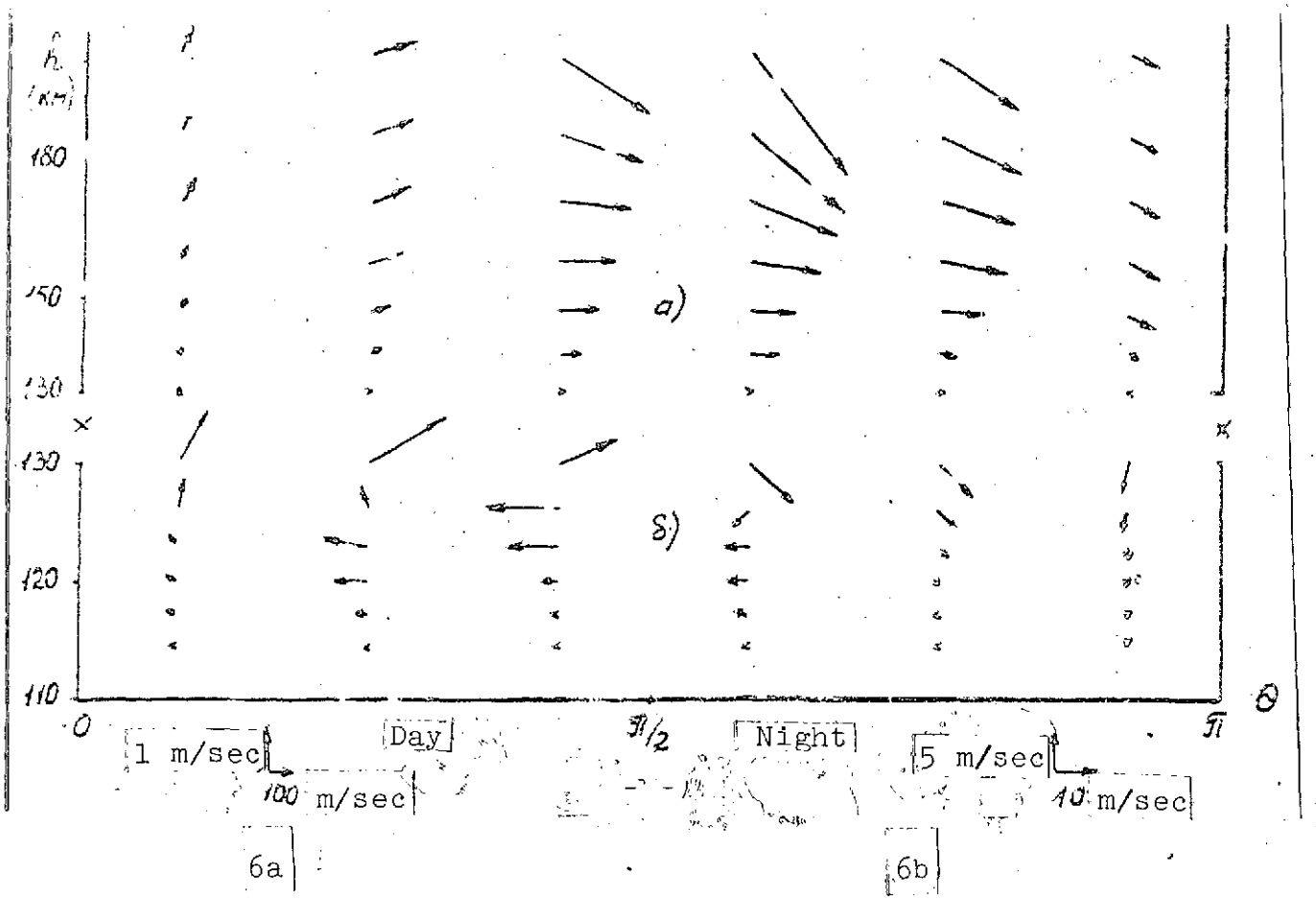

Figure 6. Wind velocity distribution in a non-rotating Venus thermosphere

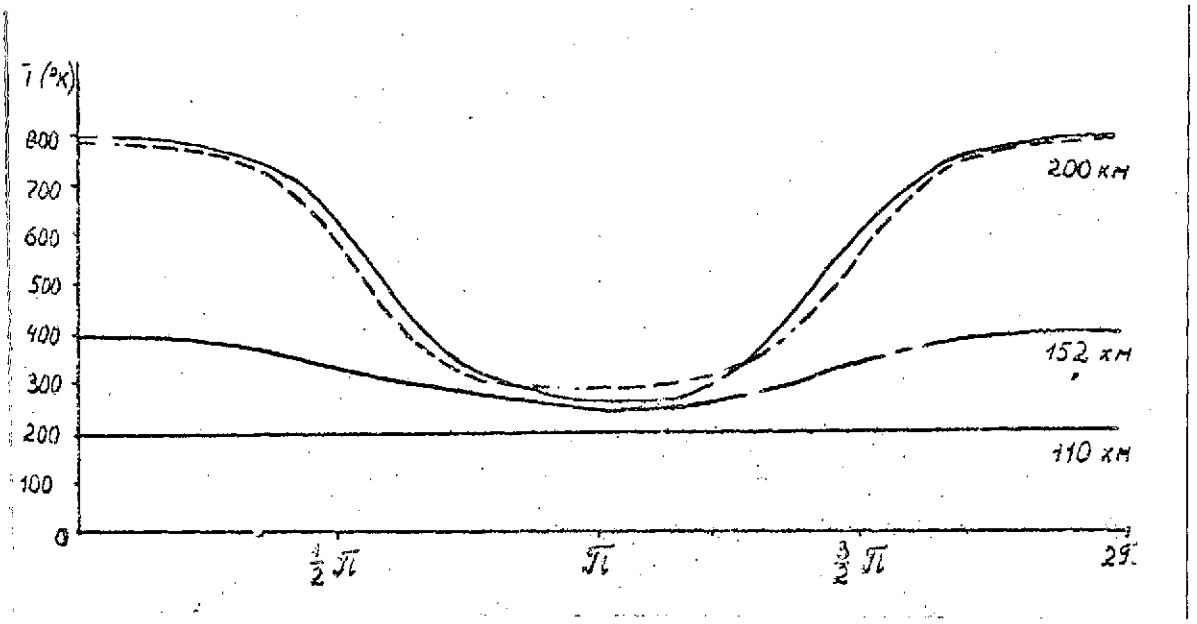

Figure 7. Temperature T distribution with angle in the equatorial region of a Venus thermosphere that rotates with a period of 4 terrestrial days (solid curve), and of a non-rotating thermosphere (broken curve).

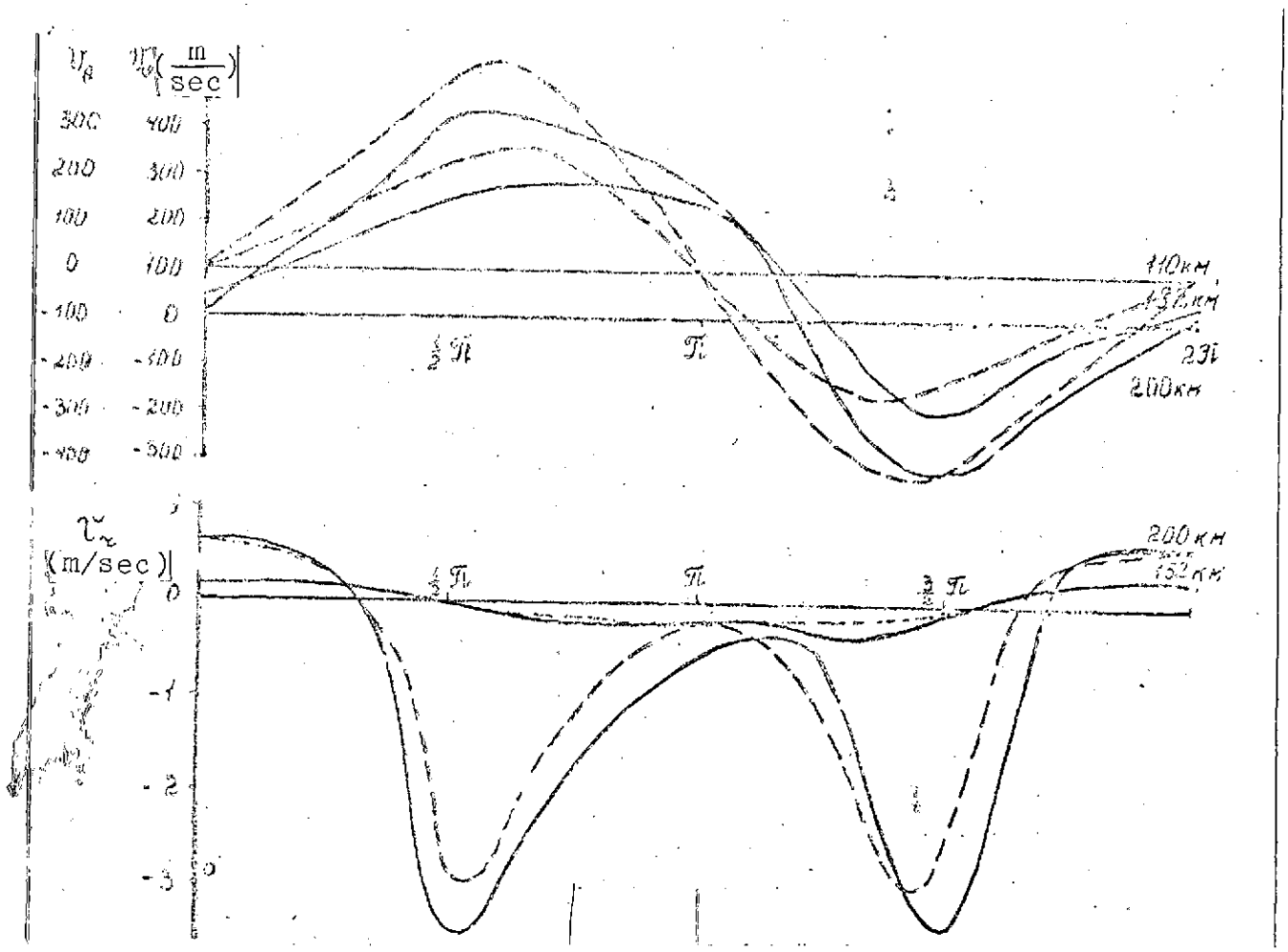

Figure 8. Distribution of the horizontal (v_ϕ) and vertical (v_r) components of the wind velocity in the equatorial region of a Venus atmosphere that rotates with a period of 4 terrestrial days (solid curve), and the corresponding components v_θ and v_r for a non-rotating thermosphere. The scale for v_θ is shifted by 100 m/sec relative to v_ϕ. Here, Ω is the angular rotation rate

REFERENCES

1. Moroz, V. I. Uspekhi fizicheskikh nauk, Vol. 104, 1971, p. 255. /21

2. Marov, M. Ya. Icarus, Vol. 16, 1972, p. 415.

3. Marov, M. Ya., V. S. Avduevsky et al. J. Atmos. Sci., 1973, p. 30.

4. Kurt, V. G., S. E. Dostovalov and E. K. Scheffer. J. Atmos. Sci., Vol. 25, 1968, p. 668.

5. Kurt, V. G., E. K. Scheffer and S. B. Dostovalov. In the book: Fizika luny i planet (Physics of the Moon and the Planets). Moscow, 1972, p. 275.

6. Barth, C. A. J. Atmos. Sci., Vol. 25, 1968, p. 564.

7. Barth, C. A. et al. Science, Vol. 158, 1967, p. 1678.

8. Barth, C. A., L. Wallace and J. B. Pearce. J. Geophys. Res., Vol. 73, 1968, p. 2541.

9. Kliore, A. et al. Science, Vol. 158, 1967, p. 1683.

10. Fjeldbo, G. and V. R. Eshleman. Radio Sci., Vol. 4, 1969, p. 879.

11. Eshleman, R. Radio Sci., Vol. 5, 1970, p. 325.

12. Rasool, S. I. and R. W. Stewart. J. Atmos. Sci., Vol. 28, 1971, p. 869.

13. Stewart, R. W. J. Atmos. Sci., Vol. 25, 1968, p. 578.

14. Stewart, R. W. J. Atmos. Sci., Vol. 28, 1971, p. 1069.

15. Moroz, V. I. and V. G. Kurt. Kosmicheskiye issledovaniya, Vol. 6, 1968, p. 577.

16. Morov, M. Ya. Doklady Akademii Nauk (DAN) SSSR, Vol. 196, 1971, p. 67.

17. Moroz, V. I. Preprint from IKI (Institute Kosmicheskikh Issledovaniy), 1973, p. 162.

18. McElroy, M. B. J. Geophys. Res., Vol. 73, 1968, p. 1513.

19. McElroy, M. B. J. Atmos. Sci., Vol. 25, 1968, p. 574.

20. McElroy, M. B. J. Geophys. Res., Vol. 74, 1969, p. 29.

21. Henry, R. J. W. and M. B. McElroy. In: "The Atmosphere of Venus and Mars", N.Y., 1968, p. 251.

22. Hogan, J. S. and P. W. Stewart. J. Atmos. Sci., Vol. 26, 1969, p. 332.

23. Donahue, T. M. J. Atmos. Sci., Vol. 25, 1968, p. 568.

24. Dickinson, R. E. J. Atmos. Sci., Vol. 28, 1971, p. 885. /22

25. Dickinson, R. E. and E. C. Ridley. J. Atmos. Sci., Vol. 29, 1972, p. 1557.

26. McElroy, M. P. Ann. Geophys., Vol. 26, 1970, p. 643.

27. Izakov, M. N. DAN SSSR, Vol. 177, 1967, p. 1324.

28. Izakov, M. N. Space Sci. Reviews, Vol. 7, 1967, p. 579.

29. Izakov, M. N. Space Sci. Reviews, Vol. 12, 1971, p. 261.

30. Izakov, M. N., S. K. Morozov and E. E. Shnol'. Preprint IKI - Pr. 115, 1972.

31. Izakov, M. N., S. K. Morozov and I. A. Yashchenko. Space Reserach, Vol. 13, 1973, p. 291.

32. Dolginov, Sh. Sh., Ye. G. Yeroshenko and L. N. Zhuzgov. Kosmicheskiye issledovaniya, Vol. 6, 1968, p. 651; Vol. 7, 1969, p. 747.

33. Bridge, H. E. et al. Science, Vol. 158, 1967, p. 1669.

34. Izakov, M. N. Geomagnetizm i aeronomiya, Vol. 10, 1970, p. 283.

35. Izakov, M. N., A. B. Dembovskiy and O. G. Lisin. Preprint, IKI, 1974.

36. Nakata, R. S. et al. Science of Light, Vol. 14, 1965, p. 54.

37. Stewart, R. W. and J. S. Hogan. J. Atmos. Sci., Vol. 26, 1969, p. 330.

38. Chamberlain, J. W. Astrophys. J., Vol. 136, 1962, p. 582.

39. Chamberlain, J. W. and M. B. McElroy. Science, Vol. 152, 1966, p. 21.

40. Dickinson, R. E. J. Atmos. Sci., Vol. 29, 1972, p. 1531.

41. Dickinson, R. E. J. Atmos. Sci., Vol. 30, 1973, p. 296.

42. Hinteregger, H. E. Ann. Geophys., Vol. 26, 1970, p. 547.

43. Ackerman, M. In: "Mesospheric Models and Related Experiments", 1971, p. 140.

44. Donahue,TT. M. J. Atmos. Sci., Vol. 28, 1971, p. 895.

45. McElroy, M. B. et al. J. Atmos. Sci., Vol. 30, 1973, p. 1437.

46. Boyer, C. Planet. Space Sci., Vol. 21, 1973, p. 1559.

47. Young, R. E. and G. Schubert. Planet. Space Sci., Vol. 21, 1973, p. 1563.

48. Broadfoot, A. L. et al. Science, Vol. 165, 1974, p. 13.

Translated for National Aeronautics and Space Administration under contract No. NASw 2483, by SCITRAN, P.O. Box 5456, Santa Barbara, California, 93108